Interaction between shock wave and single inertial bubbles near an elastic boundary

G. N. Sankin and P. Zhong*
Department of Mechanical Engineering and Materials Science, Duke University, Box 90300, Durham, North Carolina 27708, USA
(Received 9 June 2006; published 16 October 2006)

The interaction of laser-generated single inertial bubbles (collapse time=121 μs) near a silicon rubber membrane with a shock wave (55 MPa in peak pressure and 1.7 μs in compressive pulse duration) is investigated. The interaction leads to directional, forced asymmetric collapse of the bubble with microjet formation toward the surface. Maximum jet penetration into the membrane is produced during the bubble collapse phase with optimal shock wave arrival time and stand-off distance. Such interaction may provide a unique acoustic means for *in vivo* microinjection, applicable to targeted delivery of macromolecules and gene vectors to biological tissues.

DOI: 10.1103/PhysRevE.74.046304 PACS number(s): 47.55.db, 43.25.+y, 47.40.Nm

I. INTRODUCTION

Targeted delivery of macromolecules and gene vectors across biological barriers (i.e., blood vessel wall, interstitium, and cell membranes) remains to be a primary challenge for the practical applications of molecular therapy [1,2]. Among various options currently used (intravenous and parenchyma injection) or explored (electroporation and sonoporation) for targeted delivery, acoustic methods have the unique advantages of noninvasiveness and general applicability to most internal organs [3]. In particular, shock wave-inertial microbubble interaction with resultant directional microjet formation has been proposed as a unique means for *in vivo* microinjection [4,5]. Shock wave-bubble interaction and jet formation, however, depend on several attributes of the bubble, including size [6,7], oscillation phase [8], shape [9], and proximity to the boundary [6], as well as elasticity of the boundary wall [10]. Previous studies on shock wave single bubble interaction were carried out almost exclusively using gas bubbles stabilized by a plastic membrane [7] or against a gel phantom [11]. The optimal condition for shock wave inertial bubble interaction near an elastic boundary has therefore not been determined. In this paper, the interaction between lithotripter shock wave (LSW) with laser-induced single bubbles near a silicone rubber membrane surface and resultant microjet penetration into the membrane are investigated. The effects of bubble size, oscillation phase, and proximity to the boundary on the dynamics of shock wave inertial bubble interaction and jet penetration are determined.

II. MATERIALS AND METHODS

Figure 1 shows a schematic diagram of the experimental setup. A *Q*-switched Nd:YAG laser with $\lambda=1064$ nm and pulse duration 5 ns (Tempest 10, New Wave Research) was focused into a water tank ($30\times40\times15$ cm) to generate a single cavitation bubble via optical breakdown [12] at a reference time ($t=-0.2$ μs). The laser was aligned horizontally with its beam focus located 1 mm below the focal point of a piezoelectric shock wave lithotripter (FB12, Richard Wolf). At the laser focus, a typical pressure wave form of the lithotripter pulse measured by a fiber-optic probe hydrophone (FOPH-500, RP Acoustics) comprises of a leading compressive wave with a zero-crossing pulse duration of 1.7 μs, followed by a trailing tensile wave with a pulse duration of

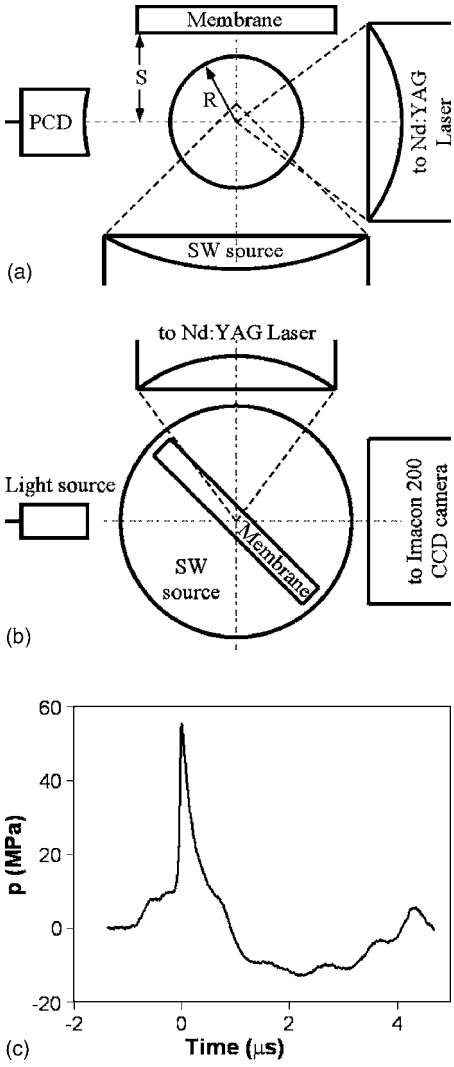

FIG. 1. Experimental setup: (a) side view, (b) top view, and (c) a representative pressure wave form at the laser focus.

*Electronic address: pzhong@duke.edu

~3 μs [see inset in Fig. 1(c)]. The positive peak pressure and the −6 dB beam diameter of the lithotripter field in this prefocal plane are 55±3 MPa and 1.8±0.2 mm, respectively.

A silicone rubber membrane (2 mm wide and 0.8 mm thick, ORON®) was placed horizontally at a stand-off distance s above the laser focus [Fig. 1(a)]. The stand-off distance can be adjusted by moving the membrane in vertical direction using a micrometer. The elastic modulus of the silicone rubber at 20% elongation is 1.3 MPa and the tensile strength is 5.5 MPa, which are similar to the elastic modulus of abdominal aorta (0.98–1.42 MPa) and femoral artery (1.23–5.50 MPa), but about 3 times of the tensile strength of artery (1.7 MPa), kidney fibrous capsule (2.3 MPa), and ureter (1.8 MPa) [13].

A high-speed imaging system (Imacon 200, DRS Hadland), in combination with a long-distance microscope (K2, Infinity) and a 5X objective lens, was used to capture the dynamics of laser-induced single bubble and LSW-bubble interaction near the silicone rubber membrane. Strobe light generated by a fiber-optic coupled flash lamp (ML-1000, Dyna-Lite) was collimated and backlit for shadowgraph imaging of shock wave propagation and jet penetration into the silicone membrane. In addition, a Xenon flash lamp (RF 300, Adapt Electronics) with a diffuser was used for visualizing the interior of the bubble. Acoustic emission (AE) from the optical breakdown in water and subsequent inertial collapse of the laser-induced bubble were measured by using a 2.25 MHz focused piezoelectric transducer (A395S, F =101.6 mm, Panametrics), connected to a digital oscilloscope (500 MHz Wave Runner 6050A, LeCroy). The collapse time (T_c) of the bubble was determined by the time delay between the first and second peaks in the AE signal. Further, an 8-channel digital delay generator (DDG 565-8C, Berkeley Nucleonics Corporation) was used to trigger the laser, the shock wave source, the flash lamp, the high-speed camera, and the oscilloscope, respectively, at selected time sequences.

In this study, laser-induced single bubbles with T_c =121 μs, which corresponds to a maximum bubble radius R_{max}=0.67 mm in free field, were used. The parameter space of the experiment was set for the nondimensionalized stand-off distance $\gamma=s/R_{max}$ to vary in the range from 0.3 to 1.2 and the normalized shock wave arrival time $\alpha=t/T_c$ in the range from 0 to 0.97.

Figure 2 depicts the vertical diameter of the laser-induced bubbles normalized by D_{max} (=$2R_{max}$), measured at different time instants (t=3–117 μs or α=0.03–0.97) and stand-off distances ($0.3<\gamma<1.2$, and $\gamma>10$). At the maximum expansion (t=60 μs), the top part of the bubble is compressed against the membrane for $\gamma<1$ (Fig. 3). Towards the end of the collapse (t=114 μs), the shape and location of the bubble can vary significantly with γ. For $\gamma<0.75$ the bubble collapses into an inverted conical shape with its base touching the membrane boundary [Fig. 4(a)], while at a slightly larger γ the bubble is separated by a layer of water from the boundary. At $\gamma\sim1$ a bubble in the form of an approximate prolate spheroid with maximal vertical diameter is observed during the collapse phase [Fig. 4(c)]. As γ increases, single bubbles of nearly spherical geometry with smaller vertical diameter are produced [10].

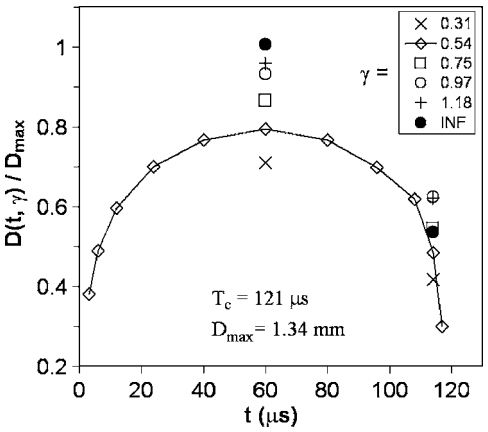

FIG. 2. Bubble vertical diameter normalized by D_{max} (=$2R_{max}$) at time t=3,6,12,24,40,60,80,96,108,114,117 μs ($\alpha=t/T_c$ =0.03,0.05,0.1,0.2,0.33,0.5,0.66,0.8,0.9,0.95,0.97), and different stand-off distance γ(0.31−∞). D_{max} is the maximum bubble diameter in free field.

III. RESULTS

The dynamics of a laser-induced single bubble oscillation near a silicone rubber membrane (γ=0.82) is shown in Fig. 3, which can be characterized primarily by bubble translation and subsequent formation of a liquid jet towards the boundary (frames 12 to 14). Figures 4(a)–4(c) compare the shock wave bubble interaction and resultant jet penetration at three different γ values (0.27, 0.75, and 1.17). In all sequences, the LSW (shown in the second frame) impinges upon the bubble near its final collapsing phase (α=0.95). Although the general features are similar to those shown in Fig. 3, the severity of the collapse is significantly enhanced. At γ=0.27 and 0.75, within two microseconds after the shock wave impact, the bubble has collapsed completely with a resultant microjet piercing through the opposite bubble wall and penetrating into the membrane [Figs. 4(a) and 4(b)]. During the collapse, the elastic boundary is attracted toward the bubble, and initiates an annular jet near the base of the conical shape bubble (frames 3–4). The initial penetration velocity of the jet in the silicon membrane is estimated to be about 150 and 200 m/s, respectively, for t =116–117 μs in Figs. 4(a) and 4(b). In comparison, at γ =1.17 the collapse of the bubble, although violent, occurs away from the membrane and, only after the rebound and during the second expansion the bubble establishes contact with the membrane [Fig. 4(c)]. It is important to note that the

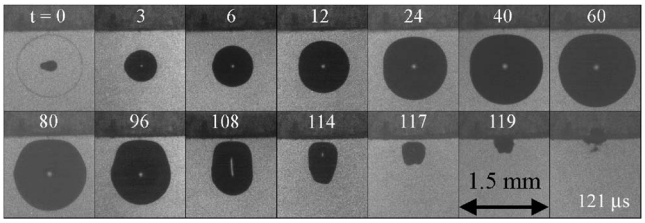

FIG. 3. Dynamics of laser-induced bubble oscillation near a silicone rubber membrane at γ=0.82. Laser light comes from the right.

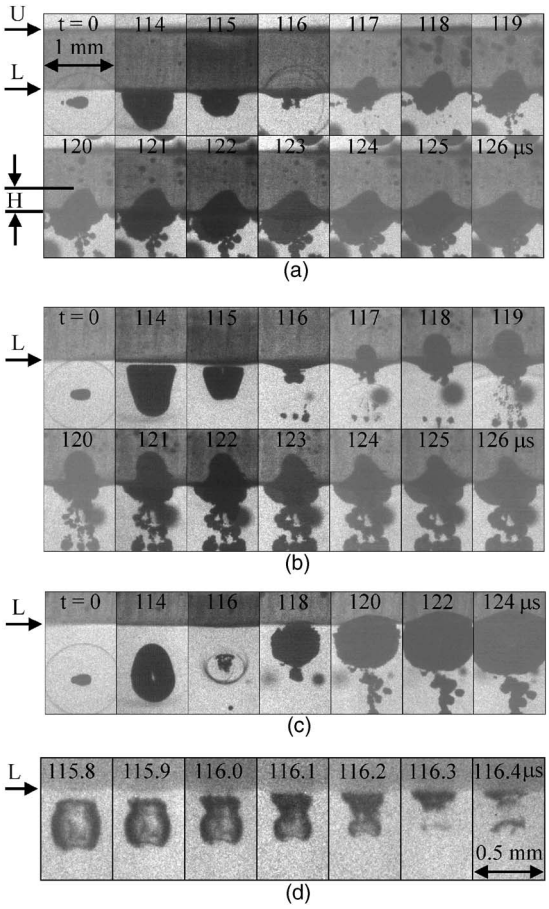

FIG. 4. Shock wave-laser induced inertial bubble interaction near a silicone rubber membrane: (a)–(c) parallel light, shock wave impinges on the bubble in the second frame, (d) diffused light. (a) γ=0.27; (b) γ=0.75; (c) γ=1.17; (d) γ=0.87. Frame width =1.0 mm in (a) to (c), 0.5 mm in (d). *L*: lower membrane surface, *U*: upper membrane surface, *H*: maximum jet penetration depth.

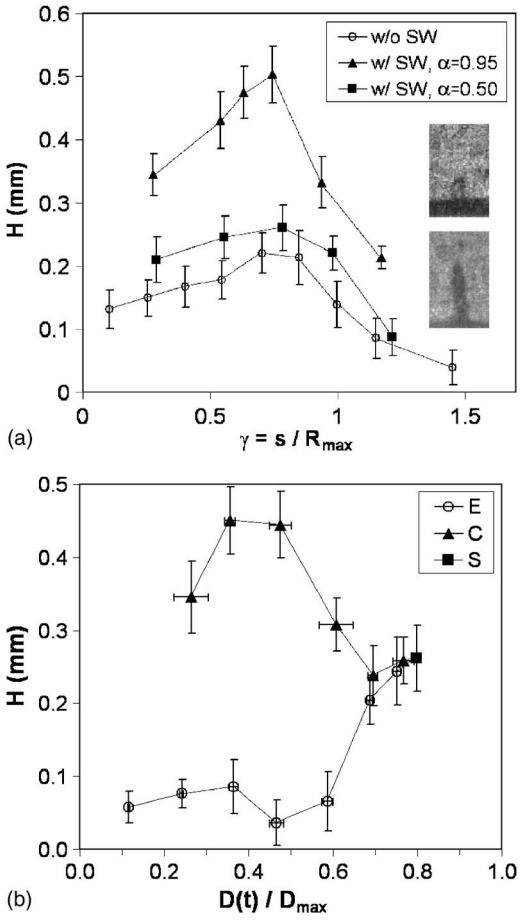

FIG. 5. Maximum jet penetration (H) produced by the shock wave bubble interaction as measured with respect to the undisturbed membrane surface; (a) effect of γ without and with shock wave (α=0.5, 0.95), inset shows residual penetration of the microjet in silicon rubber after single shot (upper), and after six shots (bottom), α=0.95, γ=0.55, frame height is 0.5 mm; (b) effect of the phase (*E*: expanding, *C*: collapsing, *S*: standing near maximum size) of bubble oscillation at different normalized shock wave arrival time t/T_c=0,0.01,0.03,0.05,0.1,0.2,0.33,0.5,0.66,0.8,0.9,0.95,0.96,0.97 (γ=0.55). D_{max} (=1.34 mm) is the maximum bubble diameter in free field. Average for three groups of measurements.

jet/bubble-membrane interaction is influenced by the trailing tensile component of the LSW, which may facilitate the expansion of the penetrated jet and rebound bubble. This assertion is supported by the observation that the maximum jet penetration depth occurs from 6 μs (γ=0.75) to 12 μs (γ =1.17) after the shock wave impact. Under diffuse illumination, the axial jet can be observed [Fig. 4(d)] to impinge upon the distal bubble wall, producing surface instability. Concomitantly, an annular jet is developed, which collapses subsequently to split the bubble into two parts [9,10,14]. Figure 5(a) shows the relationship between maximum jet penetration depth (H) in the silicon rubber membrane, measured from high-speed images [see Fig. 4(a)], and γ. The deepest penetration produced by the asymmetric collapse of the laser-generated bubble near the silicone membrane is found at γ=0.7–0.85 (open circles). It has been shown that the stronger the jet formation, the higher the collapse energy of the bubble will be carried by the jet, leading to lower secondary shock wave emission [15]. Interestingly, the deepest membrane penetration (H=0.22 mm) is observed in the proximity range (γ=0.7–0.85) where maximum jet impact velocity with minimum secondary shock wave emission has been observed [14,16]. Similarly, the deepest penetration from the LSW-inertial bubble interaction is also produced within this range (γ=0.75, solid triangles to γ=0.79, solid squares). Importantly, the penetration depth is doubled by shock wave bubble interaction near the primary collapse (α =0.95, solid triangles compared to that at the maximum expansion (α=0.5, solid squares). The inset in Fig. 5(a) shows the residual penetration of the microjet in the membrane. Furthermore, Fig. 5(b) illustrates the effect of shock wave arrival time on H for γ=0.55. In general, the value of H produced during the collapsing phase is significantly larger than its counterpart in the expanding phase, except when the interaction occurs near the maximum bubble volume [i.e., α=0.2~0.8 and $D(t)/D_{max} \geqslant 0.69$]. The maximum in H occurs during the collapsing phase at α=0.96 [$D(t)/D_{max}$ =0.36] while the minimum in H occurs during the expanding

phase at $\alpha=0.05$ $[D(t)/D_{max}=0.47]$. When the bubble is small $[D(t)/D_{max}<0.3]$, H also decreases presumably due to the small effective volume for momentum transfer during the shock wave bubble interaction [7].

IV. DISCUSSION

This work demonstrates that the dynamics of shock wave inertial–bubble interaction with resultant jet penetration into an adjacent elastic membrane depend on several important parameters, which can be described generally by $H=f(\alpha,\gamma,G_b,E)$ where G_b is a parameter representing the geometric feature of the bubble, and E is the elastic modulus of the membrane. During the shock wave bubble interaction near an elastic boundary, the force imposed on the bubble (volume$=V$) may be determined by $F_b=-V\nabla P_{SW}+F_B$ where the first term is the radiation force produced by the incident shock wave (the primary Bjerknes force) and the second term is the mutual Bjerknes force due to the effect of the boundary [17]. The interplay between these two forces determines the characteristics of the bubble dynamics, with bubble translation, asymmetric collapse, and jet formation predicted reasonably well in some cases using the concept of the Kelvin impulse [18].

The effect of α on H is similar to its effect on pressure amplification produced by shock-wave bubble interaction in free field [8]. The maximum in H is achieved when the forced collapse time of the bubble [~ 2 μs, Fig. 4(b)] matches with the compressive duration of the LSW (1.7 μs), a condition that ensures maximum momentum transfer (i.e., the work done by the LSW on the bubble, $\int pdV$, reaches a maximum). Also, when the shock wave bubble interaction occurs near the maximum bubble volume where the wall velocity is about zero, the penetration depth increases almost linearly with the bubble size [see Fig. 5(b) for $D(t)/D_{max}\geqslant 0.69$], similar to the results of shock wave interaction with a standing gas bubble ($\gamma\sim 1$) near a gel surface [11].

The effect of γ on H is influenced by several competing factors. At larger $\gamma(>1.2)$, jet impact is significantly attenuated by the interposing water layer separating the collapsing bubble and the membrane surface. As γ becomes smaller, the bubble establishes contact with the boundary during expansion and the strength of the Bjerknes attractive force increases faster than the repulsive pressure caused by the rebound of the silicone membrane surface [10]. A maximum in H is observed at $\gamma=0.7$ [Fig. 5(a), open circles] that corresponds presumably to the condition that generates maximum axial jet velocity toward the boundary. When γ is further reduced (>0.63), the shape of the bubble becomes an oblate spheroid, which enhances the collapse of the annular jet that can dampen the axial jet impact [10] and hence H. The addition of a LSW does not change the overall profile of the H-γ relation, but can significantly accelerate the axial jet impact and thus increase the penetration depth [Fig. 5(a), solid triangles].

Considering the importance of bubble shape, wall velocity, and elasticity of the boundary on jet formation [9,14], future studies are warranted to examine the shock wave inertial bubble interaction in constrained media [19], such as blood vessels and interstitial space, that are more relevant for the application of acoustic methods for targeted drug and gene delivery *in vivo*.

ACKNOWLEDGMENTS

This work was supported in part by NIH through Grant Nos. RO1-EB002682, RO1-DK52985, and S10-RR16802. The authors also acknowledge the technical support of W. Neal Simmons and Richard Wolf, GmbH, Germany for the use of the FB12 generator.

[1] R. K. Jain, Nat. Med. **4**, 655 (1998).
[2] R. Langer, Science **293**, 58 (2001).
[3] D. L. Miller, S. V. Pislaru, and J. F. Greenleaf, Somatic Cell Mol. Genet. **27**, 115 (2002).
[4] P. Zhong, H. Lin, X. F. Xi, S. L. Zhu, and E. S. Bhogte, J. Acoust. Soc. Am. **105**, 1997 (1999).
[5] C. D. Ohl and R. Ikink, Phys. Rev. Lett. **90**, 214502 (2003).
[6] Y. Tomita and A. Shima, J. Fluid Mech. **169**, 535 (1986).
[7] A. Philipp, M. Delius, C. Scheffczyk, A. Vogel, and W. Lauterborn, J. Acoust. Soc. Am. **93**, 2496 (1993).
[8] G. N. Sankin, W. N. Simmons, S. L. Zhu, and P. Zhong, Phys. Rev. Lett. **95**, 034501 (2005).
[9] O. V. Voinov and V. V. Voinov, Sov. Phys. Dokl. **21**, 133 (1976).
[10] E. A. Brujan, K. Nahen, P. Schmidt, and A. Vogel, J. Fluid Mech. **433**, 251 (2001).
[11] T. Kodama and Y. Tomita, Appl. Phys. B: Lasers Opt. **70**, 139 (2000).
[12] A. Philipp and W. Lauterborn, J. Fluid Mech. **361**, 75 (1998).
[13] F. A. Duck, *Physical Properties of Tissue: A Comprehensive Reference Book* (Academic Press, London, San Diego, 1990), p. 346.
[14] E. A. Brujan, K. Nahen, P. Schmidt, and A. Vogel, J. Fluid Mech. **433**, 283 (2001).
[15] P. Zhong, H. L. Tong, F. H. Cocks, and G. M. Preminger, J. Endourol **11**, 55 (1997).
[16] A. Vogel and W. Lauterborn, J. Acoust. Soc. Am. **84**, 719 (1988).
[17] F. R. Young, *Cavitation* (McGraw-Hill, London, 1989), p. 412.
[18] J. R. Blake, M. C. Hooton, P. B. Robinson, and R. P. Tong, Philos. Trans. R. Soc. London, Ser. A **355**, 537 (1997).
[19] P. Zhong, Y. F. Zhou, and S. L. Zhu, Ultrasound Med. Biol. **27**, 119 (2001).